**SUPPLEMENTARY INFORMATION**

# Nitrogen cycling in sediments on the NW African margin inferred from N and O isotopes in benthic chambers

A. W. Dale[a]*, D. Clemens[a], K. Dähnke[b], F. Korth[a,c], S. D. Wankel[d], U. Schroller-Lomnitz[a], K. Wallmann[a], S. Sommer[a]

[a] GEOMAR Helmholtz Centre for Ocean Research Kiel, Wischhofstrasse 1–3, 24148 Kiel, Germany

[b] Institute of Carbon Cycles, Helmholtz Centre Hereon, Max-Planck-Str. 1, 21502 Geesthacht, Germany

[c] Present address: University of Natural Resources and Life Sciences, Vienna, Peter Jordan Straße 82, 1190 Wien, Austria

[d] Department of Marine Chemistry and Geochemistry, Woods Hole Oceanographic Institution, Woods Hole, MA 02540, USA

* Corresponding author: adale@geomar.de, Tel. +49–431–600–2291, Fax +49–431–600–2928

**Isotopic composition of organic matter in shelf sediments sampled during cruise M156**

Table S1. The $\delta^{13}C$ and $\delta^{15}N$ of particulate material close to St. 5 (Station 140MUC10, 18°10.268´N, 16°31.028´W, 182 m water depth).

| Depth (cm) | $\delta^{13}C$ | $\delta^{15}N$ |
|---|---|---|
| 0.5 | -20.67 | 3.02 |
| 2.5 | -20.556 | 3.11 |
| 4.5 | -20.61 | 3.53 |
| 6.5 | -20.99 | 3.63 |
| 8.5 | -20.73 | 4.05 |
| 10.5 | -20.75 | 3.92 |
| 14.5 | -21.11 | 3.90 |
| 18.5 | -20.88 | 4.30 |
| 24.5 | -21.13 | 4.22 |
| 28.5 | -20.88 | 3.76 |

**Model of the benthic chamber incubation on the Mauritanian shelf**

*Model set-up*

The isotope model is based on a previous version for simulating N turnover in sediments and benthic chambers on the Peruvian margin (Dale et al., 2019). Dissolved species considered in the model include $O_2$, $SO_4^{2-}$, $H_2S$, total alkalinity (TA), $^{14}NO_3^-$, $^{15}NO_3^-$, $^{14}NO_2^-$, $^{15}NO_2^-$, $^{14}NH_4^+$, $^{15}NH_4^+$, $^{14}N_2$, $^{15}N_2$, $N^{16}O_3^-$, $N^{18}O_3^-$, $N^{16}O_2^-$, and $N^{18}O_2^-$. No solid species were included. Parameters are listed in Table S3, and source / sink terms in Table S4.

Organic matter degradation was parameterized as described in the main text and coupled to the reduction of $O_2$, $NO_3^-$, $NO_2^-$ and $SO_4^{2-}$ (Table S2). Ammonification was determined using the organic matter atomic C:N ratio ($r_{CN}$) in organic matter assuming a formula of $(CH_2O)(NH_3)_{1/rCN}$, where $CH_2O$ represents POC. Rate laws of AMO, NXR and AMF were parameterized as second-order reactions following previous studies (e.g. Bohlen et al., 2011). The model also includes $H_2S$ sinks via aerobic respiration ($R_{O2H2S}$, Table S2) and precipitation as particulate sulfide ($R_{H2Sp}$).

Vertical (1-D) steady-state concentrations of solutes (C) were simulated using the following reaction-transport equation assuming constant porosity (Berner, 1980; Boudreau, 1997):

$$\frac{\partial C}{\partial t} = \frac{\partial\left((D_S + D_B)\frac{\partial C}{\partial x}\right)}{\partial x} - \omega\frac{\partial C}{\partial x} + \alpha(C(0) - C) + \sum R \qquad (S1)$$

Solutes were modelled in units of µmol $cm^{-3}$ of porewater. In this equation, t (yr) is time, x (cm) is depth below the sediment–water interface, ω (cm $yr^{-1}$) is the sediment burial velocity, $D_S$ ($cm^2$ $yr^{-1}$) is the tortuosity-corrected molecular diffusion coefficient, $D_B$ ($cm^2$ $yr^{-1}$) is the bioturbation coefficient, α

is the bioirrigation coefficient ($yr^{-1}$), C(0) is the solute concentration in the bottom water, and ΣR ($\mu mol\ cm^{-3}\ yr^{-1}$) is the sum of concentration changes due to biogeochemical reactions.

Solute–specific diffusion coefficients in sediments were calculated from the temperature–dependent molecular diffusion coefficients in seawater ($D_{SW}$) and corrected for tortuosity ($\theta^2$) using the modified Weissberg equation (Boudreau, 1997; Schulz, 2000):

$$D_S = \frac{D_{SW}}{\theta^2} = \frac{D_{SW}}{1-2\ln(\varphi)} \quad (S2)$$

Differences in the diffusivity of N isotopologues are minor and were not considered (Clark and Fritz, 1997).

The decrease in bioturbation intensity with depth was described as:

$$D_B = D_B(0)\exp\left(-\frac{x^2}{2\,x_s^2}\right) \quad (S3)$$

where $D_B(0)$ is the bioturbation coefficient at the sediment–water interface and $x_s$ approximates the bioturbation halving depth.

Reasonable values were assigned to ω, $x_s$, and $D_B(0)$. The modeled solutes are insensitive to typical ranges of ω found on the margins since sediment accumulation is slow relative to diffusion (Aller, 2014). Similarly, biodiffusion coefficients are generally ~10 % or less of molecular diffusion and only relevant for the upper mixed layer. These processes are included in the model by default but could be removed without affecting the conclusions of this study.

Bioirrigation intensity, however, is important for solutes and was simulated as an exponential decrease with depth:

$$\alpha = \alpha(0)\exp\left(-\frac{x}{x_{irr}}\right) \quad (S4)$$

where α(0) is the irrigation coefficient at the sediment–water interface and $x_{irr}$ approximates the bioirrigation halving depth. The rate of bioirrigation was mainly constrained from the porewater solute concentrations.

*Isotope calculations*

The modeled processes of the N cycle involving kinetic isotope fractionations are shown in Fig. S4. The isotopic fractionation of a reactant, C, in an enzymatically mediated reaction $R_i$ was expressed using the fractionation factor, $\alpha_i$ (Rees, 1973):

$$\alpha_i = \frac{{}^{L}R_i / {}^{L}C}{{}^{H}R_i / {}^{H}C} \quad (S5)$$

where ${}^{L}R_i$ and ${}^{H}R_i$ are the rates of consumption of the light and heavy isotopes and the total rate $R_i = {}^{L}R_i + {}^{H}R_i$. ${}^{L}C$ and ${}^{H}C$ are the concentrations of the isotopes, where the total concentration $C = {}^{L}C + {}^{H}C$. The kinetic isotopic effect (${}^{H}\varepsilon$, ‰) is related to α by the expression:

$$^{H}\varepsilon_i = (\alpha_i - 1) \cdot 1000 \quad \text{(S6)}$$

The reaction rate of $^{L}C$ and $^{H}C$ in compound *j* was based on mole fractions, Φ:

$$^{L}R_i = {}^{L}\Phi_i^j \cdot R_i = \frac{\alpha_i \, {}^{L}C}{C + {}^{L}C(\alpha_i - 1)} \cdot R_i \quad \text{(S7)}$$

$$^{H}R_i = {}^{H}\Phi_i^j \cdot R_i = \frac{{}^{H}C}{\alpha_i C - {}^{H}C(\alpha_i - 1)} \cdot R_i \quad \text{(S8)}$$

Mole fractions were imposed directly if the isotope signature of the substrate (reactant) pool was assumed constant. For instance, the $^{15}N$ and $^{14}N$ mole fractions of $NH_4^+$ produced by ammonification were calculated using the (assumed constant) $\delta^{15}N$ of PON ($\delta^{15}N_{PON}$):

$$^{15}\Phi_{AMF} = \frac{1000 + \delta^{15}N_{PON}}{\delta^{15}N_{PON} + 1000 + \frac{1000}{(^{15}N/^{14}N)_{AIR}}} \quad \text{(S9)}$$

$$^{14}\Phi_{AMF} = 1 - {}^{15}\Phi_{AMF} \quad \text{(S10)}$$

Likewise, the $^{18}O$ and $^{16}O$ mole fractions of nitrite produced by AMO were determined as:

$$^{18}\Phi_{AMONO2} = \frac{1000 + \delta^{18}O_{AMONO2}}{\delta^{18}O_{AMONO2} + 1000 + \frac{1000}{(^{18}O/^{16}O)_{VSMOW}}} \quad \text{(S11)}$$

$$^{16}\Phi_{AMONO2} = 1 - {}^{18}\Phi_{AMONO2} \quad \text{(S12)}$$

where $\delta^{18}O_{AMONO2}$ is the $\delta^{18}O$ of $NO_2^-$ produced during $NH_4^+$ oxidation to $NO_2^-$:

$$\delta^{18}O_{AMONO2} = \frac{1}{2} \cdot (\delta^{18}O_2 - \epsilon_{O2}) + \frac{1}{2} \cdot \left(\delta^{18}O_{H2O} - \epsilon_{H2O\_1}\right) \quad \text{(S13)}$$

$\delta^{18}O_2$ is the $\delta^{18}O$ of ambient dissolved $O_2$ (assumed to be 23.5 ‰, Casciotti et al., 2010), $\varepsilon_{O2}$ is the KIE of $O_2$ incorporation during $NH_4^+$ oxidation to $NO_2^-$ (14 ‰, Granger and Wankel, 2016), $\delta^{18}O_{H2O}$ is the $\delta^{18}O$ of $H_2O$, and $\varepsilon_{H2O\_1}$ is the KIE of $H_2O$ incorporation during $NH_4^+$ oxidation to $NO_2^-$ (14 ‰, Casciotti et al., 2010; Granger and Wankel, 2016).

During the oxidation of $NO_2^-$ to $NO_3^-$, the additional O atom is extracted from water. The $^{18}O$ mole fraction of $NO_2^-$ consumed by nitrite oxidation ($^{18}\Phi_{NXR}^{NO2}$) was corrected for this addition using the $^{18}O$ mole fraction of water consumed during NXR ($^{18}\Phi_{NXR}^{H2O}$):

$$^{18}\Phi_{NXRNO3} = \frac{2}{3} \cdot {}^{18}\Phi_{NXR}^{NO2} + \frac{1}{3} \cdot {}^{18}\Phi_{NXR}^{H2O} \quad \text{(S14)}$$

where ${}^{18}\Phi_{NXRNO3}$ is the final mole fraction of $NO_3^-$ produced by NXR. The corresponding equation for $^{16}O$ is:

$$ {}^{16}\Phi_{NXRNO3} = \frac{2}{3} \cdot {}^{16}\Phi_{NXR}^{NO2} + \frac{1}{3} \cdot (1 - {}^{18}\Phi_{NXR}^{H2O}) \quad (S15) $$

and the $^{18}O$ mole fraction of water is:

$$ {}^{18}\Phi_{NXR}^{H2O} = \frac{\delta^{18}O_{H2O} - \epsilon_{H2O\_2} + 1000}{\delta^{18}O_{H2O} - \epsilon_{H2O\_2} + 1000 + \frac{1000}{(^{18}O/^{16}O)_{VSMOW}}} \quad (S16) $$

$\varepsilon_{H2O\_2}$ is the $^{18}O$ KIE of $H_2O$ incorporation during $NO_2^-$ oxidation to $NO_3^-$ (14 ‰, Buchwald and Casciotti, 2010). The O mole fractions for the oxidation of $NO_2^-$ to $NO_3^-$ during anammox (${}^{16}\Phi_{AMXNO3}$, ${}^{18}\Phi_{AMXNO3}$) were treated in an identical manner, using the mole fractions ${}^{16}\Phi_{AMX}^{NO2}$ and ${}^{18}\Phi_{AMX}^{NO2}$, and where ${}^{18}\Phi_{AMX}^{H2O}$=${}^{18}\Phi_{NXR}^{H2O}$.

Finally, during nitrate reduction, the extraction of O is associated with a normal kinetic isotope effect, $\epsilon_{NARBR}$. The $\delta^{18}O$ of $NO_3^-$ consumed during NAR is:

$$ \delta^{18}O_{NAR} = \frac{1000 \cdot ({}^{18}\Phi_{NAR}^{NO3} - \frac{1000}{(^{18}O/^{16}O)_{VSMOW}} + \frac{1000}{(^{18}O/^{16}O)_{VSMOW}} \cdot {}^{18}\Phi_{NAR}^{NO3})}{\frac{1000}{(^{18}O/^{16}O)_{VSMOW}} \cdot ({}^{18}\Phi_{NAR}^{NO3} - 1)} \quad (S17) $$

and the $\delta^{18}O$ of $NO_2^-$ after O extraction from $NO_3^-$ is:

$$ \delta^{18}O_{NARNO2} = \delta^{18}O_{NAR} + \varepsilon_{NARBR} \quad (S18) $$

Since $\epsilon_{NARBR}$ is positive (25 ‰, Granger and Wankel, 2016), O extraction leads to an increase in the $\delta^{18}O$ of $NO_2^-$. The final mole fractions of $^{18}O$ and $^{16}O$ of $NO_2^-$ produced during NAR are then:

$$ {}^{18}\Phi_{NARNO2} = \frac{(^{18}O/^{16}O)_{VSMOW} \cdot (1000 + \delta^{18}O_{NARNO2})}{1000 \cdot \left(1 + (^{18}O/^{16}O)_{VSMOW}\right) + \delta^{18}O_{NARNO2} \cdot (^{18}O/^{16}O)_{VSMOW}} \quad (S19) $$

$$ {}^{16}\Phi_{NARNO2} = 1 - {}^{16}\Phi_{NARNO2} \quad (S20) $$

Reaction stoichiometries are listed in Table S3.

Mole fractions of heavy isotopes in the bottom water were calculated from δ values:

$$ {}^{15}\Phi NO_{3\_BW}^- = \frac{\delta^{15}N_{NO3\_BW}}{\delta^{15}N_{NO3\_BW} + 1000 + \frac{1000}{(^{15}N/^{14}N)_{Air}}} \quad (S21) $$

$$^{15}\Phi NO_{2_{BW}}^{-} = \frac{\delta^{15}N_{NO2\_BW}}{\delta^{15}N_{NO2\_BW} + 1000 + \frac{1000}{(^{15}N/^{14}N)_{Air}}} \quad (S22)$$

$$^{15}\Phi NH_{4_{BW}}^{+} = \frac{\delta^{15}N_{NH4\_BW}}{\delta^{15}N_{NH4\_BW} + 1000 + \frac{1000}{(^{15}N/^{14}N)_{Air}}} \quad (S23)$$

$$^{15}\Phi N_{2_{BW}} = \frac{\delta^{15}N_{N2\_BW}}{\delta^{15}N_{N2\_BW} + 1000 + \frac{1000}{(^{15}N/^{14}N)_{Air}}} \quad (S24)$$

$$^{18}\Phi NO_{3\_BW}^{-} = \frac{\delta^{18}O_{NO3\_BW}}{\delta^{18}O_{NO3\_BW} + 1000 + \frac{1000}{(^{18}O/^{16}O)_{VSMOW}}} \quad (S25)$$

$$^{18}\Phi NO_{2\_BW}^{-} = \frac{\delta^{18}O_{NO2\_BW}}{\delta^{18}O_{NO2\_BW} + 1000 + \frac{1000}{(^{18}O/^{16}O)_{VSMOW}}} \quad (S26)$$

Fluxes, F (µmol cm$^{-2}$ yr$^{-1}$), of each solute, C, at the sediment surface were calculated with the model as:

$$F_C = \varphi \cdot \left(\omega \cdot C - D_S \cdot \frac{\partial C}{\partial x}\right) \quad (S27)$$

The $\delta^{15}N$ or $\delta^{18}O$ of the flux of species C, $\delta_{F_C}$, were calculated from the fluxes of the light and heavy isotopes:

$$\delta_{F_C} = \left(\frac{\left(F_{H_C}/F_{L_C}\right)}{(H/L)_{Standard}} - 1\right) \cdot 1000 \quad (S28)$$

The model was solved using the 'MethodOfLines' option by the numerical solver NDSolve in Mathematica 11 over a variable spatial grid with >700 nodes with a layer thickness increasing from 10 µm at the surface to 1 cm at the bottom. The model was run to steady-state, i.e. invariable concentrations and reaction rates with time. Mass conservation was > 99%. Fixed concentrations equal to measured bottom water values were imposed for solutes at the sediment–water interface (Table S2). At the lower boundary (12 cm), all species were prescribed a zero–gradient (Neumann) condition.

*Benthic chamber calculations*

The fluxes of each solute (Eq. (S27)) served as source/sink terms for the ordinary differential equations that describe concentration changes (dC/dt) in the benthic chambers. The units of F were converted to µmol $dm^{-3}$ $h^{-1}$ by multiplying by the factor 10/365/24/hw, where hw is the height of the water in the chamber in m. The $\delta^{15}N$ and $\delta^{18}O$ of the N species in the chamber were calculated using Eq. (1) in the main text.

In these simulations, the $H_2S$ in the chamber accumulated to several 10s of µM despite the presence of $O_2$. $H_2S$ was not measured in the chambers and we cannot verify this observation, although from previous experience we suspect that no $H_2S$ accumulated when $O_2$ is available. Therefore, we included an aerobic sink for $H_2S$ in the chamber model to remove it:

$$H_2S \text{ sink} = k \cdot H_2S \cdot O_2 \quad \text{(S29)}$$

where the rate constant for this reaction ($k = 10^3$ $\mu mol^{-1}$ $dm^3$ $h^{-1}$) was simply set to a high enough level to remove the excess $H_2S$. $O_2$ loss inside the chamber was assumed to be $2 \cdot k \cdot H_2S \cdot O_2$.

Table S2. Reaction network used in the model.

| Stoichiometry | Rate expression [a,b] |
|---|---|
| POM degradation by oxygen reduction, $R_{O2POC}$:<br>$(CH_2O)(NH_3)_{1/rCN} + O_2 \rightarrow (1 - r_{CN}^{-1})\ CO_2 +$<br>$r_{CN}^{-1}\ HCO_3^- + r_{CN}^{-1}NH_4^+ + (1 - r_{NC}^{-1})H_2O$ | $R_{O2POC} = f_{O_2} \cdot RPOC$, where $\begin{cases} f_{O_2} = 1 \text{ for } [O_2] \geq K_{O2POC} \\ f_{O_2} = \dfrac{[O_2]}{K_{O2POC}} \text{ for } [O_2] \leq K_{O2POC} \end{cases}$ |
| POM degradation by nitrite reduction, $R_{NIR}$:<br>$(CH_2O)(NH_3)_{1/rCN} + 4/3\ NO_2^- + (1/3 + r_{NC}^{-1})CO_2 \rightarrow$<br>$2/3\ N_2 + (4/3 + r_{CN}^{-1})HCO_3^- + r_{CN}^{-1}NH_4^+ + (1/3 - r_{CN}^{-1})H_2O$ | $R_{NIR} = f_{NO_2} \cdot RPOC$, where $\begin{cases} f_{NO_2} = 0 \text{ for } f_{O_2} = 1 \\ f_{NO_2} = (1 - f_{O_2}) \text{ for } f_{O_2} < 1 \text{ and } [NO_2^-] > K_{NIR} \\ f_{NO_2} = (1 - f_{O_2}) \dfrac{[NO_2^-]}{K_{NIR}} \text{ for } f_{O_2} < 1 \text{ and } [NO_2^-] \leq K_{NIR} \end{cases}$ |
| POM degradation by nitrate reduction, $R_{NAR}$:<br>$(CH_2O)(NH_3)_{1/rCN} + 2\ NO_3^- \rightarrow 2\ NO_2^- + (1 - r_{CN}^{-1})\ CO_2 +$<br>$r_{CN}^{-1}\ HCO_3^- + r_{CN}^{-1}NH_4^+ + (1 - r_{NC}^{-1})H_2O$ | $R_{NAR} = f_{NO_3} \cdot RPOC$, where $\begin{cases} f_{NO_3} = 0 \text{ for } f_{NAR} \equiv f_{O_2} + f_{NO_2} = 1 \\ f_{NO_3} = (1 - f_{NAR}) \text{ for } f_{NAR} < 1 \text{ and } [NO_3^-] > K_{NAR} \\ f_{NO_3} = (1 - f_{NAR}) \dfrac{[NO_3^-]}{K_{NAR}} \text{ for } f_{NAR} < 1 \text{ and } [NO_3^-] \leq K_{NAR} \end{cases}$ |
| POM degradation by sulfate reduction, $R_{SR}$:<br>$(CH_2O)(NH_3)_{1/rCN} + 0.5\ SO_4^{2-} + r_{CN}^{-1}CO_2 +$<br>$r_{CN}^{-1}H_2O \rightarrow 0.5\ H_2S + (1 + r_{CN}^{-1})HCO_3^- + r_{CN}^{-1}NH_4^+$ | $R_{SR} = (1 - f_{O_2} - f_{NO_2} - f_{NO_3}) \cdot RPOC$ |
| Ammonium oxidation, $R_{AMO}$:<br>$NH_4^+ + 1.5O_2 \rightarrow NO_2^- + H_2O + 2H^+$ | $R_{AMO} = k_{AMO} \cdot [O_2] \cdot [NH_4^+]$ |
| Nitrite oxidation, $R_{NXR}$:<br>$NO_2^- + 0.5O_2^- \rightarrow NO_3^-$ | $R_{NXR} = k_{NXR} \cdot [O_2] \cdot [NO_2^-]$ |
| Anammox, $R_{AMX}$ [a]:<br>$NH_4^+ + 1.3\ NO_2^- \rightarrow N_2 + 0.3\ NO_3^- + 2\ H_2O$ | $R_{AMX} = k_{AMX} \cdot [NO_2^-] \cdot [NH_4^+]$ |
| Sulfide oxidation, $R_{O2H2S}$:<br>$H_2S + 2\ O_2 \rightarrow SO_4^{2-} + 2H^+$ | $R_{O2H2S} = k_{O2H2S} \cdot [O_2] \cdot [H_2S]$ |
| Particulate sulphide precipitation, $R_{H2Sp}$:<br>$H_2S \rightarrow S(s)$ | $R_{H2Sp} = k_{H2Sp} \cdot [H_2S] \cdot \exp(-5 \cdot x)$ |
| Ammonification, $R_{AMF}$:<br>Organic N $\rightarrow NH_4^+$ | $R_{AMF} = RPOC / r_{CN}$ |

[a] Anammox reaction stoichiometry is unbalance with regards to the transfer of electrons. As described by Brunner et al. (2013), excess $NO_3^-$ production is balanced by the reduction of inorganic carbon during production of biomass.

Table S3. Model parameters used for the benthic chamber incubation experiment at St. 2 on the shelf (BIGO 2-5). Results from this model are shown in Fig. 4 in the main text.

| Term | Description | Value [a] |
|---|---|---|
| L | Length of simulated sediment column (cm) | 12 |
| T | Bottom water temperature, ($^{o}$C) | 15 |
| S | Bottom water salinity, (-) | 35 |
| $\varphi$ | Sediment porosity, (–) | 0.8 |
| $\omega_L$ | Sediment burial velocity, (cm yr$^{-1}$) | 0.07 |
| $D_B(0)$ | Bioturbation coefficient at sediment surface, (cm$^2$ yr$^{-1}$) | 5 |
| $x_s$ | Bioturbation depth parameter, (cm) | 2 |
| $\alpha(0)$ | Bio-irrigation coefficient at x=0, (yr$^{-1}$) | 1500 |
| $x_{irr}$ | Bio-irrigation attenuation parameter (cm) | 1.5 |
| $D_{SW\_O2}$ | Diffusion coefficient in seawater of $O_2$ (cm$^2$ yr$^{-1}$) | 477 |
| $D_{SW\_NO3}$ | Diffusion coefficient in seawater of $NO_3^-$ (cm$^2$ yr$^{-1}$) | 495 |
| $D_{SW\_NO2}$ | Diffusion coefficient in seawater of $NO_2^-$ (cm$^2$ yr$^{-1}$) | 452 |
| $D_{SW\_SO4}$ | Diffusion coefficient in seawater of $SO_4^{2-}$ (cm$^2$ yr$^{-1}$) | 264 |
| $D_{SW\_NH4}$ | Diffusion coefficient in seawater of $NH_4^+$ (cm$^2$ yr$^{-1}$) | 495 |
| $D_{SW\_N2}$ | Diffusion coefficient in seawater of $N_2$ (cm$^2$ yr$^{-1}$) | 418 |
| $D_{SW\_H2S}$ | Diffusion coefficient in seawater of $H_2S$ (cm$^2$ yr$^{-1}$) | 436 |
| $D_{SW\_TA}$ | Diffusion coefficient in seawater of TA (cm$^2$ yr$^{-1}$) [b] | 290 |
| $k_{O2H2S}$ | Rate constant for $H_2S$ oxidation, ($\mu$mol$^{-1}$ cm$^3$ yr$^{-1}$) | $1.0\times10^6$ |
| $k_{AMO}$ | Rate constant for $NH_4^+$ oxidation, ($\mu$mol$^{-1}$ cm$^3$ yr$^{-1}$) | Table 3 in main text |
| $k_{NXR}$ | Rate constant for $NO_2^-$ oxidation, ($\mu$mol$^{-1}$ cm$^3$ yr$^{-1}$) | Table 3 in main text |
| $k_{H2Sp}$ | Rate constant for $H_2S$ precipitation as particulate S, (yr$^{-1}$) | $1.0\times10^6$ |
| $K_{O2POC}$ | Threshold constant for $O_2$ for POC degradation, ($\mu$mol cm$^{-3}$) [c] | 0.002 |
| $K_{NAR}$ | Threshold constant for $NO_3^-$ for POC degradation, ($\mu$mol cm$^{-3}$) | Table 3 in main text |
| $K_{NIR}$ | Threshold constant for $NO_2^-$ for POC degradation, ($\mu$mol cm$^{-3}$) | Table 3 in main text |
| $r_{CN}$ | Atomic C:N ratio of organic matter, (mol C / mol N) | 0.050 |
| $O_{2\_BW}$ | Bottom water $O_2$ concentration, ($\mu$mol cm$^{-3}$) | 0.035 |
| $NO_3^-{}_{BW}$ | Bottom water $NO_3^-$ concentration, ($\mu$mol cm$^{-3}$) | 0.025 |
| $NO_2^-{}_{BW}$ | Bottom water $NO_2^-$ concentration, ($\mu$mol cm$^{-3}$) | 0.0001 |
| $SO_4^{2-}{}_{BW}$ | Bottom water $SO_4^{2-}$ concentration, ($\mu$mol cm$^{-3}$) | 28 |
| $NH_4^+{}_{BW}$ | Bottom water $NH_4^+$ concentration, ($\mu$mol cm$^{-3}$) | $1.0\times10^{-7}$ |
| $N_{2\_BW}$ | Bottom water $N_2$ concentration, ($\mu$mol cm$^{-3}$) [d] | 0.520 |
| $H_2S_{BW}$ | Bottom water $H_2S$ concentration, ($\mu$mol cm$^{-3}$) | 0 |
| $TA_{BW}$ | Bottom water TA concentration, ($\mu$mol cm$^{-3}$) | 2.332 |
| $\delta^{18}O_{H2O}$ | $\delta^{18}$O of ambient seawater, (‰) | 0 |
| $\delta^{18}O_{O2}$ | $\delta^{18}$O of ambient dissolved oxygen, (‰) | 23.5 |
| $\epsilon_{O2}$ | KIE of $O_2$ incorporation during $NH_4^+$ oxidation to $NO_2^-$, (‰) | 14 |
| $\epsilon_{H2O\_1}$ | KIE of $H_2O$ incorporation during $NH_4^+$ oxidation to $NO_2^-$, (‰) | 14 |
| $\epsilon_{H2O\_2}$ | KIE of $H_2O$ incorporation during $NO_2^-$ oxidation to $NO_3^-$, (‰) | 14 |
| $\delta^{15}N_{PON}$ | $\delta^{15}$N of PON, (‰) | 5 |
| $\delta^{18}O_{AMONO2}$ | $\delta^{18}$O of $NO_2^-$ produced from the oxidation of $NH_4^+$, (‰) | -2.3 (Eq. S13) |
| $\epsilon_{NARBR}$ | KIE of O extraction from $NO_3^-$ during NAR, (‰) | 25 |
| $^{15}\epsilon_{NAR}$ | N KIE for $NO_3^-$ by NAR, (‰) | Table 3 in main text |
| $^{18}\epsilon_{NAR}$ | O KIE for $NO_3^-$ by NAR, (‰) | Table 3 in main text |
| $^{15}\epsilon_{NIR}$ | N and O KIE for $NO_2^-$ by NIR, (‰) | Table 3 in main text |
| $^{18}\epsilon_{NIR}$ | O KIE for $NO_2^-$ by NIR, (‰) | Table 3 in main text |
| $\epsilon_{AMO}$ | N KIE for $NH_4^+$ by AMO, (‰) | Table 3 in main text |
| $^{15}\epsilon_{NXR}$ | N KIE for $NO_2^-$ by NXR, (‰) | Table 3 in main text |
| $^{18}\epsilon_{NXR}$ | O KIE for $NO_2^-$ by NXR, (‰) | Table 3 in main text |
| $\delta^{15}N_{NH4\_BW}$ | $\delta^{15}$N of $NH_4^+$ in the bottom water, (‰) [d] | 5 |
| $\delta^{15}N_{NO3\_BW}$ | $\delta^{15}$N of $NO_3^-$ in the bottom water, (‰) | 5.2 |
| $\delta^{15}N_{NO2\_BW}$ | $\delta^{15}$N of $NO_2^-$ in the bottom water, (‰) [d] | 0 |
| $\delta^{15}N_{N2\_BW}$ | $\delta^{15}$N of $N_2$ in the bottom water, (‰) [d] | 0 |
| $\delta^{18}O_{NO3\_BW}$ | $\delta^{18}$O of $NO_3^-$ in the bottom water, (‰) | 4.1 |
| $\delta^{18}O_{NO2\_BW}$ | $\delta^{18}$O of $NO_2^-$ in the bottom water, (‰) [d] | 0 |
| $^{15}NO_3^-{}_{BW}$ | Bottom water $^{15}NO_3^-$ concentration, ($\mu$mol cm$^{-3}$) | $^{15}\Phi NO_3^-{}_{BW} \cdot NO_3^-{}_{BW}$ |

| | | |
|---|---|---|
| $^{14}NO_3^-{}_{BW}$ | Bottom water $^{14}NO_3^-$ concentration, (μmol $cm^{-3}$) | $NO_3^-{}_{BW} - {}^{15}NO_3^-{}_{BW}$ |
| $^{15}NO_2^-{}_{BW}$ | Bottom water $^{15}NO_2^-$ concentration, (μmol $cm^{-3}$) | $^{15}\Phi NO_2^-{}_{BW} \cdot NO_2^-{}_{BW}$ |
| $^{14}NO_2^-{}_{BW}$ | Bottom water $^{14}NO_2^-$ concentration, (μmol $cm^{-3}$) | $NO_2^-{}_{BW} - {}^{15}NO_2^-{}_{BW}$ |
| $^{15}NH_4^-{}_{BW}$ | Bottom water $^{15}NH_4^-$ concentration, (μmol $cm^{-3}$) | $^{15}\Phi NH_4^-{}_{BW} \cdot NH_4^-{}_{BW}$ |
| $^{14}NH_4^-{}_{BW}$ | Bottom water $^{14}NH_4^-$ concentration, (μmol $cm^{-3}$) | $NH_4^-{}_{BW} - {}^{15}NH_4^-{}_{BW}$ |
| $^{15}N_2^-{}_{BW}$ | Bottom water $^{15}N_2^-$ concentration, (μmol $cm^{-3}$) | $^{15}\Phi N_2^-{}_{BW} \cdot N_2^-{}_{BW}$ |
| $^{14}N_2^-{}_{BW}$ | Bottom water $^{14}N_2^-$ concentration, (μmol $cm^{-3}$) | $N_2^-{}_{BW} - {}^{15}N_2^-{}_{BW}$ |
| $^{18}NO_3^-{}_{BW}$ | Bottom water $^{18}NO_3^-$ concentration, (μmol $cm^{-3}$) | $^{18}\Phi NO_3^-{}_{BW} \cdot NO_3^-{}_{BW}$ |
| $^{16}NO_3^-{}_{BW}$ | Bottom water $^{16}NO_3^-$ concentration, (μmol $cm^{-3}$) | $NO_3^-{}_{BW} - {}^{18}NO_3^-{}_{BW}$ |
| $^{18}NO_2^-{}_{BW}$ | Bottom water $^{18}NO_2^-$ concentration, (μmol $cm^{-3}$) | $^{18}\Phi NO_2^-{}_{BW} \cdot NO_2^-{}_{BW}$ |
| $^{16}NO_2^-{}_{BW}$ | Bottom water $^{16}NO_2^-$ concentration, (μmol $cm^{-3}$) | $NO_2^-{}_{BW} - {}^{18}NO_2^-{}_{BW}$ |

[a] Parameter values measured directly or inferred from other data unless otherwise indicated.
[b] Diffusion coefficient for TA was set equal to that for bicarbonate ion ($HCO_3^-$), which typically comprises >95% of DIC in porewater.
[c] Jourabchi et al. (2005)
[d] Assumed (bottom water $N_2$ concentration)

Table S4. Rate expressions applied in the differential equations (ΣR in Eq. (S1)).

| Variable | ΣR |
|---|---|
| $^{14}NO_3^-$ | $-2 \cdot {}^{14}\Phi_{NAR}^{NO3} \cdot R_{NAR} + {}^{14}\Phi_{NXR}^{NO2} \cdot R_{NXR} + 0.3 \cdot {}^{14}\Phi_{AMX}^{NO2} \cdot R_{AMX}$ |
| $^{15}NO_3^-$ | $-2 \cdot {}^{15}\Phi_{NAR}^{NO3} \cdot R_{NAR} + {}^{15}\Phi_{NXR}^{NO2} \cdot R_{NXR} + 0.3 \cdot {}^{15}\Phi_{AMX}^{NO2} \cdot R_{AMX}$ |
| $^{14}NO_2^-$ | $+{}^{14}\Phi_{AMO}^{NH4} \cdot R_{AMO} + 2 \cdot {}^{14}\Phi_{NAR}^{NO3} \cdot R_{NAR} - \frac{4}{3} \cdot {}^{14}\Phi_{NIR}^{NO2} \cdot R_{NIR} - {}^{14}\Phi_{NXR}^{NO2} \cdot R_{NXR} - 1.3 \cdot {}^{14}\Phi_{AMX}^{NO2} \cdot R_{AMX}$ |
| $^{15}NO_2^-$ | $+{}^{15}\Phi_{AMO}^{NH4} \cdot R_{AMO} + 2 \cdot {}^{15}\Phi_{NAR}^{NO3} \cdot R_{NAR} - \frac{4}{3} \cdot {}^{15}\Phi_{NIR}^{NO2} \cdot R_{NIR} - {}^{15}\Phi_{NXR}^{NO2} \cdot R_{NXR} - 1.3 \cdot {}^{15}\Phi_{AMX}^{NO2} \cdot R_{AMX}$ |
| $^{14}NH_4^+$ | $+{}^{14}\Phi_{AMF} \cdot R_{AMF} - {}^{14}\Phi_{AMO}^{NH4} \cdot R_{AMO} - {}^{14}\Phi_{AMX}^{NH4} \cdot R_{AMX}$ |
| $^{15}NH_4^+$ | $+{}^{15}\Phi_{AMF} \cdot R_{AMF} - {}^{15}\Phi_{AMO}^{NH4} \cdot R_{AMO} - {}^{15}\Phi_{AMX}^{NH4} \cdot R_{AMX}$ |
| $^{14}N_2$ | $+0.5 \cdot \left(\frac{4}{3} \cdot {}^{14}\Phi_{NIR}^{NO2} \cdot R_{NIR} + {}^{14}\Phi_{AMX}^{NO2} \cdot R_{AMX} + {}^{14}\Phi_{AMX}^{NH4} \cdot R_{AMX}\right)$ |
| $^{15}N_2$ | $+0.5 \cdot \left(\frac{4}{3} \cdot {}^{15}\Phi_{NIR}^{NO2} \cdot R_{NIR} + {}^{15}\Phi_{AMX}^{NO2} \cdot R_{AMX} + {}^{15}\Phi_{AMX}^{NH4} \cdot R_{AMX}\right)$ |
| $^{16}NO_3^-$ | $-2 \cdot {}^{16}\Phi_{NAR}^{NO3} \cdot R_{NAR} + {}^{16}\Phi_{NXRNO3} \cdot R_{NXR} + 0.3 \cdot {}^{16}\Phi_{AMXNO3} \cdot R_{AMX}$ |
| $^{18}NO_3^-$ | $-2 \cdot {}^{18}\Phi_{NAR}^{NO3} \cdot R_{NAR} + {}^{18}\Phi_{NXRNO3} \cdot R_{NXR} + 0.3 \cdot {}^{18}\Phi_{AMXNO3} \cdot R_{AMX}$ |
| $^{16}NO_2^-$ | $+\delta^{16}O_{AMONO2} \cdot R_{AMO} + 2 \cdot {}^{16}\Phi_{NARNO2} \cdot R_{NAR} - \frac{4}{3} \cdot {}^{16}\Phi_{NIR}^{NO2} \cdot R_{NIR} - {}^{16}\Phi_{NXR}^{NO2} \cdot R_{NXR} - {}^{16}\Phi_{AMX}^{NO2} \cdot R_{AMX} - 0.3 \cdot {}^{16}\Phi_{AMXNO3} \cdot R_{AMX}$ |
| $^{18}NO_2^-$ | $+\delta^{18}O_{AMONO2} \cdot R_{AMO} + 2 \cdot {}^{18}\Phi_{NARNO2} \cdot R_{NAR} - \frac{4}{3} \cdot {}^{18}\Phi_{NIR}^{NO2} \cdot R_{NIR} - {}^{18}\Phi_{NXR}^{NO2} \cdot R_{NXR} - {}^{18}\Phi_{AMX}^{NO2} \cdot R_{AMX} - 0.3 \cdot {}^{18}\Phi_{AMXNO3} \cdot R_{AMX}$ |
| $O_2$ | $- R_{O2POC} - 2 \cdot R_{O2H2S} - 1.5 \cdot R_{AMO} - 0.5 \cdot R_{NXR}$ |
| $SO_4^{2-}$ | $- 0.5 \cdot R_{SO4POC} + R_{O2H2S}$ |
| $H_2S$ | $+ 0.5 \cdot R_{SO4POC} - R_{O2H2S} - R_{H2Sp}$ |
| TA | $r_{CN} \cdot R_{POC} + 4/3 \cdot R_{NIR} + R_{SO4POC} - 2 \cdot R_{AMO} + 2 \cdot R_{O2H2S}$ |

Table S5. Isotope results from the benthic incubations (see text for details). For each station, the data from both BIGO chambers were combined. Uncertainties (±) on $^{15}\varepsilon_{app}$ and O $^{18}\varepsilon_{app}$ represent the standard error of the regression slopes, whilst those for $\delta^{15}$N-$NH_4$ are the standard error of the intercept ($r^2$ values of the slopes are given in brackets). Uncertainties (±) on $^{18}\varepsilon_{app}$ : $^{15}\varepsilon_{app}$ were calculated using standard error propagation rules. Only significant results ($p < 0.05$) are shown. Mean ± standard deviation is also given.

| Station | Water depth (m) | $^{15}\varepsilon_{app}$ (‰) | $^{18}\varepsilon_{app}$ (‰) | $^{18}\varepsilon_{app}$:$^{15}\varepsilon_{app}$ (-) | $\delta J_{NH4}$ (‰) |
|---|---|---|---|---|---|
| 1 | 46 | 1.0 ± 0.2 (0.77) | 2.0 ± 0.6 (0.55) | 2.0 ± 0.3 | 8.0 ± 2.6 (0.81) |
| 2 | 65 | 0.7 ± 0.1 (0.71) | 1.6 ± 0.2 (0.82) | 2.3 ± 0.2 | 9.6 ± 0.5 (0.15) |
| 3 | 90 | 1.6 ± 0.2 (0.88) | | | 9.3 ± 3.4 (0.50) |
| 4 | 130 | 1.4 ± 0.4 (0.45) | 2.9 ± 0.2 (0.92) | 2.0 ± 0.3 | |
| 5 | 174 | 1.8 ± 0.5 (0.53) | 1.7 ± 0.7 (0.35) | 0.9± 0.5 | |
| 6 | 241 | 2.0 ± 0.3 (0.78) | 1.7 ± 0.5 (0.44) | 0.9 ± 0.3 | |
| 7 | 412 | 1.7 ± 0.6 (0.36) | | | |
| | | | | | |
| Mean | | 1.5 | 2.0 | 1.8 | 9.0 |
| SD | | 0.4 | 0.5 | 0.5 | 0.6 |

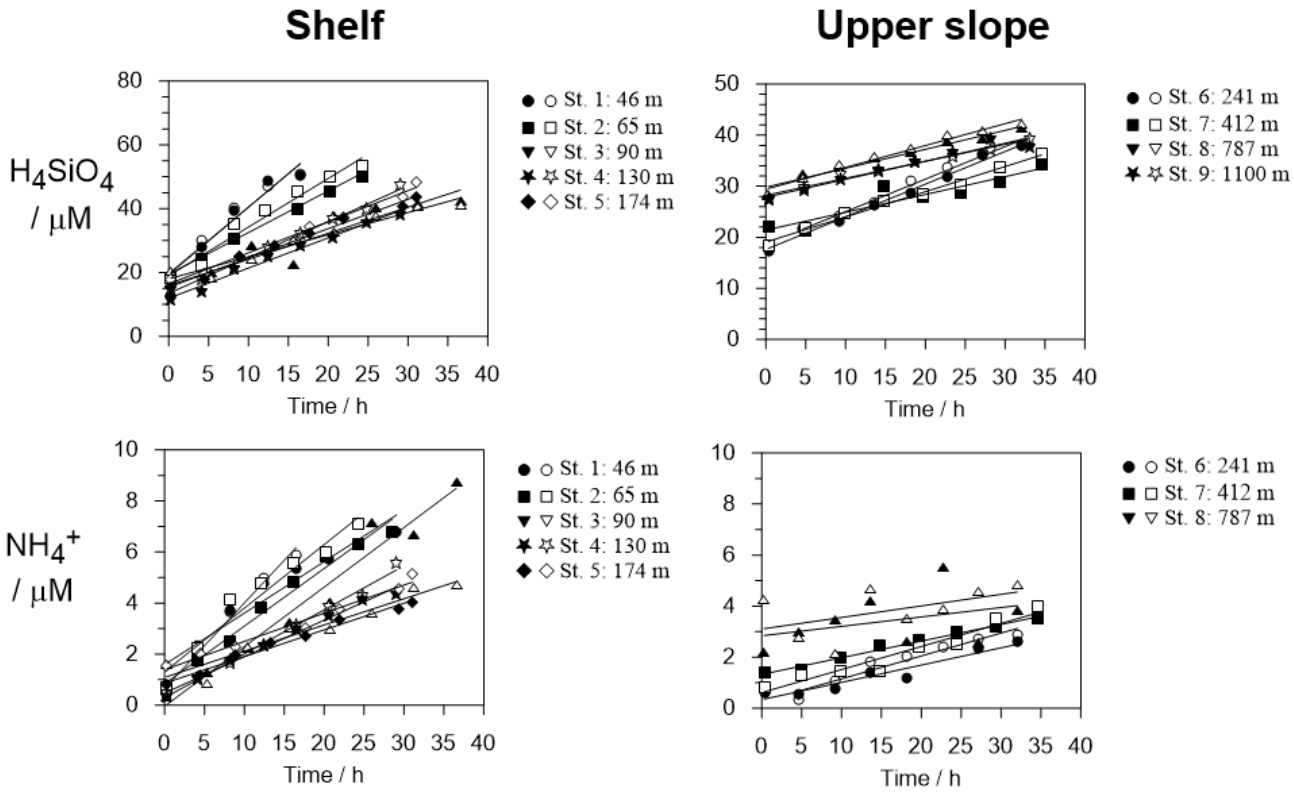


Fig. S1. Benthic chamber incubation results for $H_4SiO_4$ and $NH_4^+$ on the shelf and upper slope. Plots show linear regression curves from which the fluxes are calculated Open and filled symbols correspond to chamber 1 and 2 during each BIGO lander deployment, respectively. Accompanying $PO_4^{3-}$ and DIC data have been reported by Schroller-Lomnitz et al. (2019).

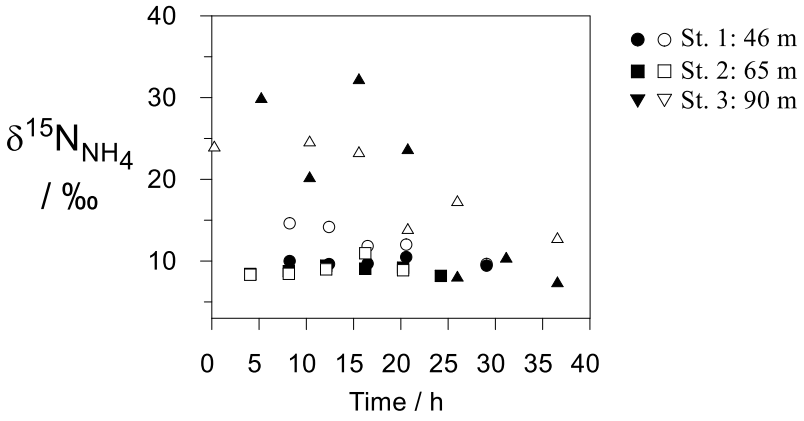


Fig. S2. Benthic chamber $\delta^{15}N\text{-}NH_4$ data for St. 1 to 3. Open and filled symbols correspond to chamber 1 and 2 during each BIGO lander deployment, respectively.

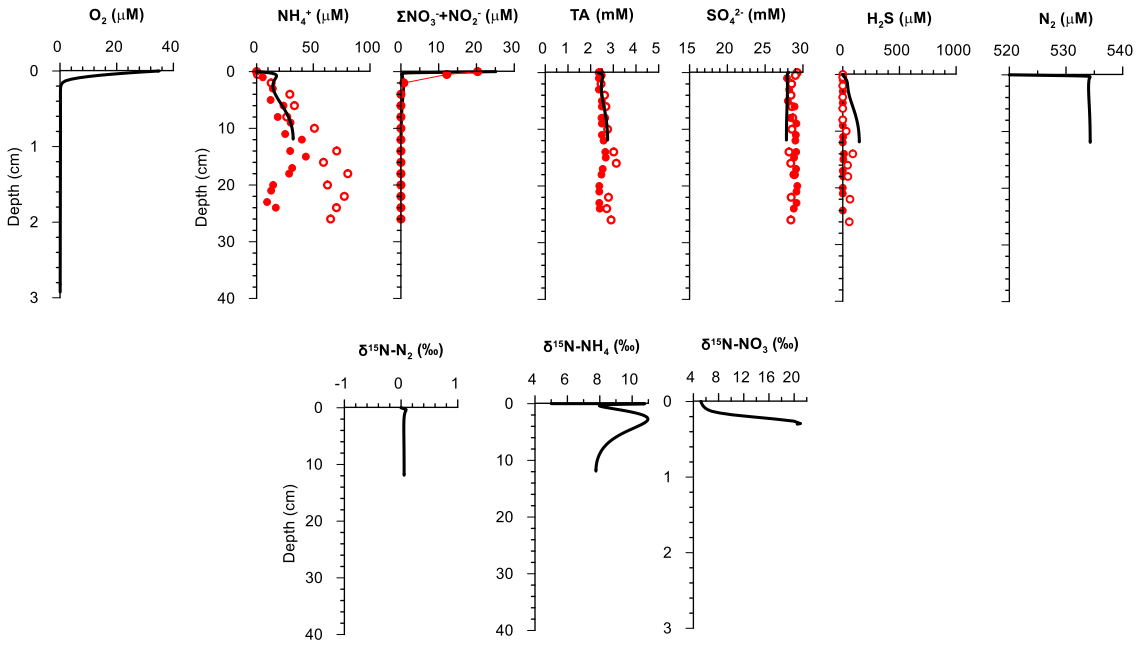


Fig. S3. Modeled (curves) and measured (open red circle: St. 1; red full: St. 2) porewater profiles for the shallow shelf. The modelled profiles are one of 54 examples from the Monte-Carlo fit to the chamber data. See main text for more information.

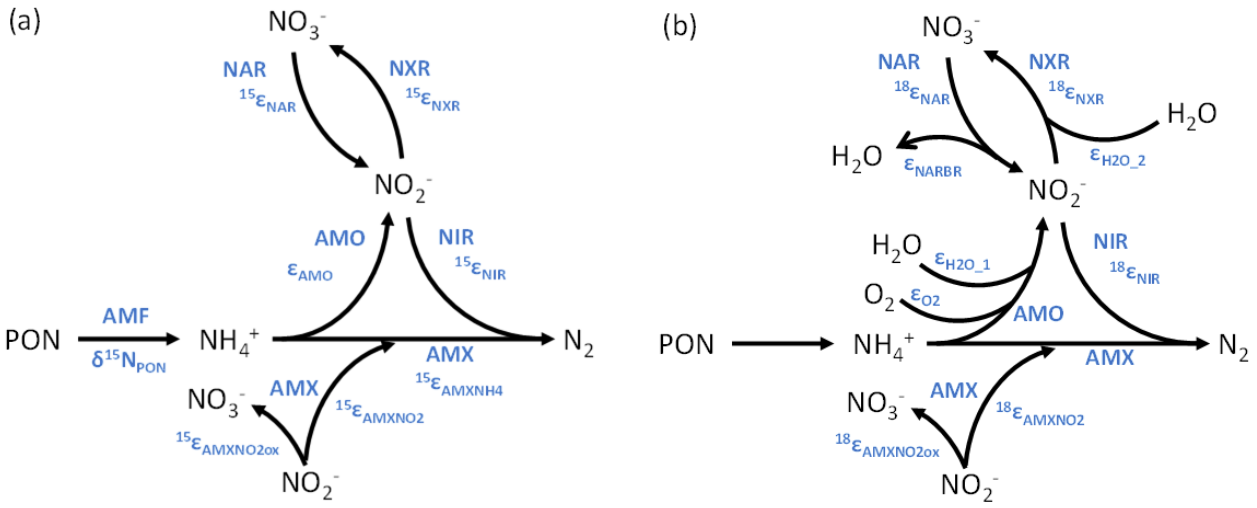


Fig. S4. Conceptual model of the N transformation pathways considered in the model that affect (a) $\delta^{15}N$ and (b) $\delta^{18}O$, after Granger and Wankel (2016). See text for more information.

**References**


Aller R.C. (2014) Sedimentary Diagenesis, Depositional Environments, and Benthic Fluxes. In: Holland H.D. and Turekian K.K. (eds.) *Treatise on Geochemistry*, Second Edition, vol. 8, pp. 293-334. Oxford: Elsevier.

Berner R. A. (1980) Early Diagenesis: A Theoretical Approach, Princeton University Press, Princeton.

Bohlen, L., Dale, A. W., Sommer, S., Mosch, T., Hensen, C., Noffke, A., Scholz, F., and Wallmann, K. (2011) Benthic nitrogen cycling traversing the Peruvian oxygen minimum zone. *Geochim. Cosmochim. Acta* 75, 6094–6111.

Boudreau B. P. (1997) Diagenetic models and their implementation, Springer-Verlag, Berlin.

Brunner B., Contreras S., Lehmann M. F., Matantseva O., Rollog M., Kalvelage T., Klockgether G., Lavik G., Jetten M. S. M., Kartal B. and Kuypers M. M. M. (2013) Nitrogen isotope effects induced by anammox bacteria. Proc. Natl. Acad. Sci. U. S. A. 110, 18994-18999.

Buchwald C. and Casciotti K. L. (2010) Oxygen isotopic fractionation and exchange during bacterial nitrite oxidation. *Limnol. Oceanogr.* 55, 1064–1074.

Casciotti, K. L., McIlvin, M. R., and Buchwald, C. (2010) Oxygen isotopic exchange and fractionation during bacterial ammonia oxidation. *Limnol. Oceanogr.* 55, 753–762.

Clark I. D. and Fritz P. (1997) Environmental Isotopes in Hydrogeology, CRC Press, Boca Raton, Louisiana.

Dale, A.W., Bourbonnais, A., Altabet, M., Wallmann, K. and Sommer, S. (2019) Isotopic fingerprints of benthic nitrogen cycling in the Peruvian oxygen minimum zone. *Geochim. Cosmochim. Acta* 245, 406-425.

Granger, J., and Wankel, S. D. (2016) Environmental overprinting of nitrate isotopes. *Proc. Nat. Acad. Sci.* 113 (42) E6391-E6400; DOI: 10.1073/pnas.1601383113

Jourabchi, P., Van Cappellen, P. and Pierre Regnier (2005) Quantitative interpretation of pH distributions in aquatic sediments: A reaction-transport modeling approach. *Am. J. Sci.*, 305 919-956.

Rees C. E. (1973) A steady-state model for sulphur isotope fractionation in bacterial reduction processes. Geochim. Cosmochim. Acta 37, 1141–1162.

Schroller-Lomnitz, U., Hensen, C., Dale, A. W., Scholz, F., Clemens, D., Sommer., S, Noffke, A., Wallmann, K. (2019) Dissolved benthic phosphate, iron and carbon fluxes in the Mauritanian upwelling system and implications for ongoing deoxygenation. *Deep-Sea Res. I* 143, 70-84.

Schulz, H. D. (2000) Conceptual models and computer models, in *Marine Geochemistry*, edited by H. D. Schulz and M. Zabel, pp 417-442, Springer-Verlag, Berlin.